THE JOURNAL OF BIOLOGICAL CHEMISTRY VOL. 291, NO. 8, pp. 3747–3756, February 19, 2016

Mechanism of Ribonucleotide Incorporation by Human DNA Polymerase η*

Received for publication, November 24, 2015, and in revised form, January 5, 2016 Published, JBC Papers in Press, January 6, 2016, DOI 10.1074/jbc.M115.706226

Yan Su, Martin Egli, and F. Peter Guengerich[1]

From the Department of Biochemistry, Vanderbilt University School of Medicine, Nashville, Tennessee 37232-0146

Ribonucleotides and 2′-deoxyribonucleotides are the basic units for RNA and DNA, respectively, and the only difference is the extra 2′-OH group on the ribonucleotide sugar. Cellular rNTP concentrations are much higher than those of dNTP. When copying DNA, DNA polymerases not only select the base of the incoming dNTP to form a Watson-Crick pair with the template base but also distinguish the sugar moiety. Some DNA polymerases use a steric gate residue to prevent rNTP incorporation by creating a clash with the 2′-OH group. Y-family human DNA polymerase η (hpol η) is of interest because of its spacious active site (especially in the major groove) and tolerance of DNA lesions. Here, we show that hpol η maintains base selectivity when incorporating rNTPs opposite undamaged DNA and the DNA lesions 7,8-dihydro-8-oxo-2′-deoxyguanosine and cyclobutane pyrimidine dimer but with rates that are 10^3-fold lower than for inserting the corresponding dNTPs. X-ray crystal structures show that the hpol η scaffolds the incoming rNTP to pair with the template base (dG) or 7,8-dihydro-8-oxo-2′-deoxyguanosine with a significant propeller twist. As a result, the 2′-OH group avoids a clash with the steric gate, Phe-18, but the distance between primer end and Pα of the incoming rNTP increases by 1 Å, elevating the energy barrier and slowing polymerization compared with dNTP. In addition, Tyr-92 was identified as a second line of defense to maintain the position of Phe-18. This is the first crystal structure of a DNA polymerase with an incoming rNTP opposite a DNA lesion.

RNA and DNA are fundamental to life in all forms. The two nucleic acid polymers are composed of ribonucleotides and 2′-deoxyribonucleotides as the basic units, respectively. However, ribonucleotides have been found in DNA; they constitute a large proportion of the "DNA lesions" in the genome. In mice, they have been shown to be collectively the most frequently occurring DNA lesions, even more than abasic sites and 7,8-dihydro-8-oxo-2′-deoxyguanosine (8-oxodG).[2] The presence of ribonucleotides in DNA increases the possibility of spontaneous hydrolysis, causing DNA to break more frequently. These ribonucleotides are mainly removed from DNA by the RNase H2 pathway (1–5).

DNA polymerases introduce ribonucleotides into DNA by misinserting them (6). Concentrations of cellular rNTPs are 1–6 orders of magnitude higher than those of dNTPs, depending on the cell type and the stage of the cell cycle (6–9). To discriminate dNTP from rNTP, a steric gate residue (typically a tyrosine or phenylalanine) is generally conserved in DNA polymerases and thought to create a clash with the extra hydroxyl group of the incoming rNTP (10–17). Although limited in extent, ribonucleotide incorporation has still been observed by a variety of DNA polymerases, from replicative ones with relatively high fidelity and small active sites (*e.g.* pol ϵ and pol δ) to error-prone X-family pol λ and pol β and Y-family pol ι (6, 8, 17–21).

Compared with other DNA polymerases, those in the Y-family are known for high misinsertion rates and tolerance of DNA adducts in the template strand by relying on their spacious active sites (22–24). Y-family human DNA polymerase η (hpol η) is of particular interest, as it is the only known DNA polymerase directly related to a human genetic disorder, mainly due to its unique role in translesion synthesis past the UV-induced DNA lesion cyclobutane pyrimidine dimer (CPD). Patients defective in hpol η, the result of which is a form of xeroderma pigmentosum (XP-V), are typically highly sensitive to UV light, with increased incidence of skin and other types of cancer and (for some of the individuals) neurodegeneration (25–28). hpol η is also involved in translesion synthesis of other DNA lesions, *e.g.* 8-oxodG (29, 30), abasic sites (31, 32), and cisplatin or other therapeutic drug-induced DNA damage (33–38).

In this study, we investigated the ability of hpol η to incorporate ribonucleotides into DNA and crystallized hpol η with incoming rNTPs opposite both undamaged DNA and an 8-oxodG lesion. Our results demonstrate that hpol η can incorporate ribonucleotides into DNA with relatively high selectivity but low efficiency, even when the template strand contains the DNA lesion 8-oxodG or CPD. The x-ray crystal structures show that the incoming rNTP at the hpol η active site adopts a slightly different orientation relative to dNTP to avoid a clash with the steric gate residue, without significantly disrupting the pairing with the template dG or 8-oxodG. The latter appears to be the first crystal structure of an incoming rNTP opposite a DNA lesion within a DNA polymerase.

* This work was supported, in whole or in part, by National Institutes of Health Grants R01 ES010375 (to F. P. G. and M. E.), R01 ES010546 (to F. P. G.), and P01 CA160032 (to M. E.). The authors declare that they have no conflicts of interest with the contents of this article. The content is solely the responsibility of the authors and does not necessarily represent the official views of the National Institutes of Health.

The atomic coordinates and structure factors (codes 5EWE, 5EWF, and 5EWG) have been deposited in the Protein Data Bank (http://wwpdb.org/).

[1] To whom correspondence should be addressed: Dept. of Biochemistry, Vanderbilt University School of Medicine, 638B Robinson Research Bldg., 2200 Pierce Ave., Nashville, TN 37232-0146. Tel.: 615-322-2261; Fax: 615-343-0704; E-mail: f.guengerich@vanderbilt.edu.

[2] The abbreviations used are: 8-oxodG, 7,8-dihydro-8-oxo-2′-deoxyguanosine; h, human; pol, DNA polymerase; CPD, cyclobutane pyrimidine dimer; PDB, Protein Data Bank; dAMPNPP, 2′-deoxyadenosine-5′-[(α,β)-imido]-triphosphate; dCMPNPP, 2′-deoxycytidine-5′-[(α,β)-imido]triphosphate.

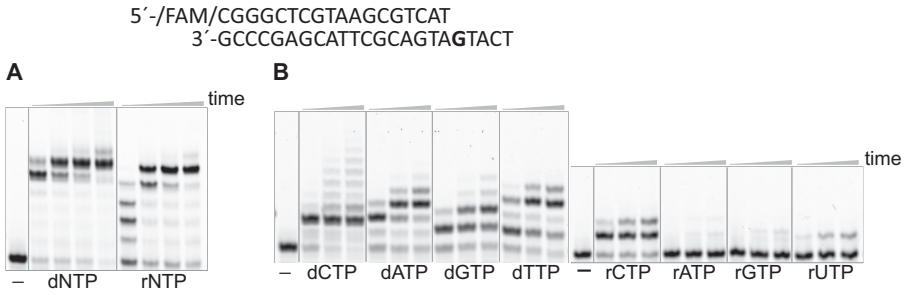

FIGURE 1. **hpol η incorporates dNTPs or rNTPs opposite an unmodified DNA template.** *A*, full-length extension of the primer opposite unmodified DNA template (5 μM) with all four dNTPs or rNTPs by hpol η (1.2 μM) at 37 °C for 5, 30, 55, and 240 min (time gradients depicted with *wedges*). *B*, single nucleotide incorporation assays with 5 μM native primer-template DNA substrate, 500 nM hpol η, and 1 mM each of individual dNTP or rNTP at 37 °C for 5, 30, and 55 min.

Experimental Procedures

Materials—Oligonucleotides were purchased from Integrated DNA Technologies (Coralville, IA) or TriLink BioTechnologies (San Diego) and purified by HPLC by the manufacturers. rNTPs and dNTPs were purchased from New England Biolabs (Ipswich, MA). These experiments were conducted with the catalytic core of hpol η or the Y92A mutant (1–432 amino acids), and the former has been shown to have similar catalytic activity as the full-length protein *in vitro* (33). The hpol η and the Y92A mutant (1–432 amino acids) were expressed and purified as reported previously (39). Polyethylene glycol monomethyl ether 2000 (from Hampton Research, Aliso Viejo, CA) was used for crystallization.

DNA Substrates—The fluorescently labeled primer 5′-6-carboxyfluorescein-CGG GCT CGT AAG CGT CAT-3′ was annealed with each of the following template oligonucleotides at a 1:1 molar ratio by heating to 95 °C and slowly cooling: 1) 5′-TCA TGA TGA CGC TTA CGA GCC CG-3′; 2) 5′-TCA TTA TGA CGC TTA CGA GCC CG-3′; 3) 5′-TCA T(*8-oxodG*)A TGA CGC TTA CGA GCC CG-3′; 4) 5′-TCA (*CPD*)A TGA CGC TTA CGA GCC CG-3′ (CPD indicates *cis-syn* thymine dimer). These annealed fluorescent substrates were used in extension, single nucleotide incorporation, and steady-state kinetic assays. The following oligonucleotides were annealed at equal molar ratios for crystallization: 5′-AGC GTC AT-3′ and 5′-CAT GAT GAC GCT-3′; 5′-AGC GTC AT-3′ and 5′-CAT (*8-oxodG*)AT GAC GCT-3′.

Extension, Single Nucleotide Incorporation, and Steady-state Kinetic Assays—The extension assays were conducted with 5 μM DNA substrate (oligonucleotide), 1.2 μM hpol η, and 4 mM dNTP or rNTP mixtures (1 mM for each dNTP or rNTP) in 40 mM Tris-HCl buffer (pH 7.5) containing 10 mM dithiothreitol (DTT), 0.1 mg/ml bovine serum albumin (BSA), 5% glycerol (v/v), 5 mM $MgCl_2$, and 100 mM KCl at 37 °C for 5, 30, 55, and 240 min. Single nucleotide incorporation assays were conducted using the same reaction buffer but with 5 μM annealed DNA substrate, 500 nM hpol η, and 1 mM each of dNTP or rNTP at 37 °C for 5, 30, and 55 min.

For steady-state kinetic assays, 5 μM DNA substrate was incubated with 1.5 to 500 nM hpol η or the Y92A mutant as well as varying concentrations of each dNTP or rNTP at 37 °C for 5 min, in the same reaction buffer as extension and single base incorporation assay. Reactions were stopped by the addition of a quench buffer (90% formamide (v/v) and 10 mM EDTA). Products were separated on 18% (w/v) denaturing polyacrylamide gels and visualized using a Typhoon system (GE Healthcare). The data for steady-state kinetic assays were fit to a (hyperbolic) Michaelis-Menten equation using Prism software (GraphPad, La Jolla, CA).

Crystallization, Diffraction, Data Collection, and Structure Determination—Each DNA substrate and hpol η were mixed at a molar ratio of 1.1 to 1, before adding $CaCl_2$ (final concentration 3.33 mM) and excess amount of rNTP. To obtain crystals by hanging drop vapor diffusion, 1 μl of each protein/DNA mixture was mixed with 1 μl of reservoir solution, which contained 100 mM sodium MES (pH 6.0), 5 mM $CaCl_2$, and 16–22% (w/v) polyethylene glycol monomethyl ether 2000, followed by equilibration with 500 μl of the reservoir solution at 18 °C. The crystals were washed through cryoprotectant (composed of 3 volumes of reservoir solution and 1 volume of glycerol) before flash freezing in liquid nitrogen. Diffraction data were collected on the 21-ID-F or 21-ID-G beamline at the Advanced Photon Source (Life Sciences Collaborative Access Team, Argonne National Laboratory, Argonne, IL). Data were integrated and scaled using HKL2000 (40), processed with Phaser MR (41) for molecular replacement phasing (PDB code 4O3N as the search model for hpol η·dG·rCTP, and PDB code 4O3P for hpol η·dG·rCTP and hpol η·dG·rATP) (29), and refined with PHENIX (42). Model building was performed with ARP/ω ARP classic (43, 44) and COOT (45). All illustrations were generated with the program UCSF Chimera (46).

Results

hpol η Inserts Ribonucleotides Opposite Undamaged Template dG or dA—To assess the ribonucleotide incorporation ability of hpol η, we compared the extension of the primers in the presence of all four dNTPs or rNTPs with different incubation times. The primer was extended at 5 min and reached full-length after 30 min in the presence of rNTPs, compared with 5 min for full-length extension with dNTPs (Fig. 1*A*). To estimate the fidelity of ribonucleotide incorporation, hpol η was incubated with annealed undamaged DNA substrate as well as individual dNTP or rNTP. Under our reaction conditions, multiple nucleotides were added to the primer in the presence of a single dNTP in an error-prone manner. However, only one or two nucleotide extensions was observed with a single rNTP. Among the four ribonucleotides, rCTP (able to Watson-Crick pair with template dG) was the most efficient one for insertion (Fig. 1*B*).

TABLE 1
Steady-state kinetics for insertion of nucleoside triphosphates opposite dG and dT by hpol η

Template	dNTP/rNTP	K_m	k_{cat}	k_{cat}/K_m	f^a	$1/f^b$
		μM	min^{-1}	$\mu M^{-1}\ min^{-1}$		
dG	dCTP	2.4 ± 0.3	119 ± 3	50 ± 6	1	1
	dATP	84 ± 9	11 ± 1	0.13 ± 0.02	0.0026	380
	dGTP	58 ± 7	12 ± 1	0.21 ± 0.03	0.0042	240
	dTTP	170 ± 16	58 ± 2	0.34 ± 0.03	0.0068	150
	rCTP	188 ± 14	12 ± 1	0.064 ± 0.007	0.0013	770
dT	dCTP	127 ± 8	19 ± 1	0.15 ± 0.01	0.0048	210
	dATP	2.5 ± 0.2	77 ± 2	31 ± 3	1	1
	dGTP	9.1 ± 0.6	27 ± 1	3.0 ± 0.2	0.097	10
	dTTP	132 ± 15	27 ± 1	0.20 ± 0.02	0.0065	150
	rATP	278 ± 37	2.5 ± 0.1	0.0090 ± 0.0012	0.00029	3400

[a] Misinsertion frequency is as follows: $f = (k_{cat}/K_m)_{incorrect}/(k_{cat}/K_m)_{correct}$.
[b] Fold change is $1/f$.

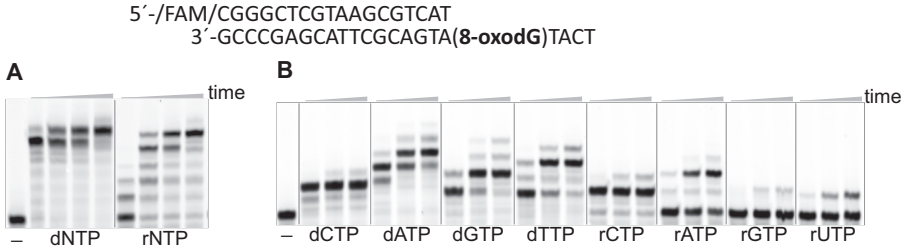

FIGURE 2. **hpol η can bypass an 8-oxodG lesion and incorporate dNTPs or rNTPs.** *A*, hpol η (1.2 μM) extended the primer against DNA template (5 μM) containing an 8-oxoG lesion in the presence of all four dNTPs or rNTPs at 37 °C for 5, 30, 55, and 240 min (time gradients depicted with *wedges*). *B*, single nucleotide incorporation assays with hpol η (500 nM) with 5 μM DNA substrate with 8-oxoG in the template and 1 mM each of dNTP or rNTP at 37 °C for 5, 30, and 55 min.

TABLE 2
Steady-state kinetics for insertion of nucleoside triphosphates opposite 8-oxodG by hpol η

Template	dNTP/rNTP	K_m	k_{cat}	k_{cat}/K_m	f	$1/f$
		μM	min^{-1}	$\mu M^{-1}\ min^{-1}$		
8-oxodG	dCTP	1.7 ± 0.3	81 ± 3	48 ± 9	1	1
	dATP	8.4 ± 1.0	77 ± 3	9.2 ± 1.1	0.19	5.3
	dGTP	18 ± 2	29 ± 1	1.6 ± 0.2	0.033	30
	dTTP	140 ± 11	44 ± 1	0.31 ± 0.03	0.0065	150
	rCTP	292 ± 42	6.1 ± 0.3	0.021 ± 0.003	0.00044	2300
	rATP	445 ± 40	0.51 ± 0.02	0.0011 ± 0.0001	0.000023	43000

To further measure the efficiency and fidelity of rNTP incorporation by hpol η, steady-state kinetic experiments were conducted. The catalytic efficiency (k_{cat}/K_m) for rCTP insertion opposite template dG was 770-fold less than that for dCTP and 2–5-fold less relative to those for the mismatched dNTPs. However, rates of incorporation of the other ribonucleotides (other than rCTP) were very low and could not be measured experimentally. In addition, to investigate the effect of the template base, another set of DNA substrates with dT in the template instead of dG was included in the steady-state kinetic study. The change for catalytic efficiency between rATP and dATP insertion opposite template dT was 3400-fold, slightly higher than that between rCTP and dCTP opposite dG (770-fold, Table 1).

hpol η Inserts Ribonucleotides Opposite 8-oxodG—We conducted primer extension assays by hpol η with 8-oxodG in the template strand in the presence of dNTPs or rNTPs. The pattern for primer extension past 8-oxodG was very similar to that against undamaged DNA (Figs. 1*A* and 2*A*). The primer was partially extended to full length by 30 min with the mixture of all four rNTPs, whereas hpol η elongated the primer to full length within 5 min with dNTPs. In single nucleotide insertion assays, only one rC was added to the primer within 5 min, although in the presence of the other individual rNTPs significantly elongated primers were only observed after 30 min of incubation (Fig. 2, *A* and *B*).

In steady-state kinetic assays, hpol η incorporated dCTP opposite template 8-oxodG 2300-fold more efficiently than rCTP and 43,000-fold more than rATP. The difference between the catalytic efficiencies for rCTP and rATP incorporation was about 19, compared with 5 for dCTP and dATP, indicating that during nucleotide incorporation hpol η has similar base selectivity regardless of the sugar (Table 2).

hpol η Incorporates Ribonucleotides Opposite CPD—Given that hpol η is capable of bypassing CPD by inserting the correct nucleotide dA (26, 28), we investigated the incorporation of ribonucleotides against this lesion. hpol η extended the primer past CPD in a manner similar to that observed opposite undamaged DNA or 8-oxodG. With only rATP, more than 50% of the primers were elongated by two nucleotides after 5 min, much faster than with the other single rNTPs (Fig. 3, *A* and *B*). Quantitatively, rATP insertion was 1400-fold less efficient than dATP opposite CPD (Table 3).

hpol η Scaffolds the Incoming rCTP and Template dG to Form a Watson-Crick Base Pair with a Propeller Twist—To understand the mechanism of ribonucleotide insertion by hpol η, we

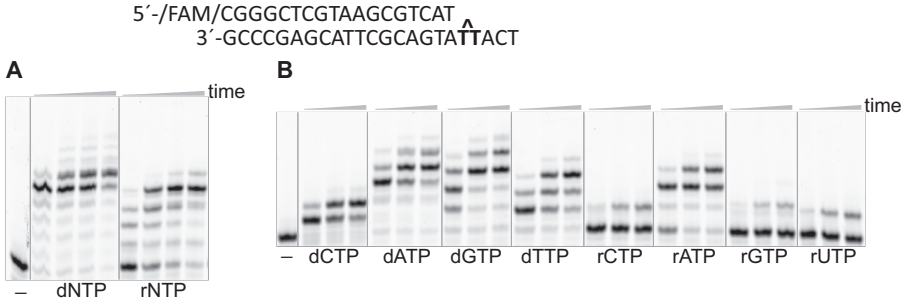

FIGURE 3. **hpol η can incorporate ribonucleotides opposite the CPD lesion and further extend the primer.** *A*, extension of the primer opposite a DNA template (5 μM) containing a CPD lesion by hpol η (1.2 μM) in the presence of all four dNTPs or rNTPs at 37 °C for 5, 30, 55, and 240 min (time gradients depicted with *wedges*). *B*, extension of the primer by incubation of 5 μM DNA substrate with a CPD in the template strand, 500 nM hpol η, and 1 mM each of individual dNTP or rNTP at 37 °C for 5, 30, and 55 min.

TABLE 3
Steady-state kinetics for insertion of nucleoside triphosphates opposite CPD by hpol η

Template	dNTP/rNTP	K_m	k_{cat}	k_{cat}/K_m	f	$1/f$
		μM	min^{-1}	$\mu M^{-1} min^{-1}$		
CPD	dCTP	31 ± 3	27 ± 1	0.87 ± 0.09	0.026	38
	dATP	1.7 ± 0.2	57 ± 1	34 ± 4	1	1
	dGTP	34 ± 3	40 ± 1	1.2 ± 0.1	0.035	29
	dTTP	23 ± 2	32 ± 1	1.4 ± 0.1	0.041	24
	rATP	295 ± 35	7.0 ± 0.3	0.024 ± 0.003	0.00071	1400

TABLE 4
Crystal data, data collection parameters, and structure refinement statistics

Complex	hpol η·dG:rCTP	hpol η·(8-oxodG):rCTP	hpol η·(8-oxodG):rATP
Data collection			
Wavelength (Å)	0.97856	0.97872	0.97856
Space group	$P6_1$	$P6_1$	$P6_1$
Resolution (Å)	50.00-1.66 (1.69-1.66)[a]	50.00-1.78 (1.81-1.78)	50.00-1.75 (1.78-1.75)
Unit cell $a = b$, c (Å)	99.28, 81.90	99.12, 81.38	99.02, 81.57
Unique reflections	54,114 (2700)	43,104 (2117)	45,786 (2302)
Completeness (%)	100.0 (100.0)	99.2 (99.1)	99.8 (100.0)
$I/\sigma(I)$	19.2 (2.4)	18.5 (1.9)	21.1 (2.2)
Wilson B-factor (Å^2)	16.8	21.6	28.1
R-merge[b]	0.098 (0.978)	0.115 (1.229)	0.086 (0.909)
Redundancy	8.9 (8.8)	8.8 (7.8)	8.5 (7.3)
Refinement			
R-work	0.1714 (0.2757)	0.1795 (0.2739)	0.1781 (0.2766)
R-free	0.2074 (0.3021)	0.2158 (0.3040)	0.2150 (0.2778)
No. of atoms			
Protein/DNA	3376/409	3304/453	3303/390
rNTP/Ca^{2+}	29/2	29/1	31/1
H_2O/glycerol	444/12	410/6	374/0
Protein residues	427	425	425
B-factor (Å)			
Average	22.2	27.0	33.4
Protein/DNA	20.5/25.7	25.8/30.7	32.2/37.8
rNTP/Ca^{2+}	16.3/17.3	19.5/15.6	29.7/23.6
Water/glycerol	31.7/24.8	33.4/20.4	39.1/-
Root mean square deviations			
Bonds (Å)	0.007	0.008	0.007
Angles (°)	1.007	1.146	1.023
Ramachandran			
Favored (%)	97.3	97.2	97.9
Allowed (%)	2.47	2.07	1.83
Outliers (%)	0.22	0.69	0.23
PDB code	5EWE	5EWF	5EWG

[a] Data shown in parentheses are from the highest resolution shell.
[b] R-merge is R linear = SUM(ABS($I - \langle I \rangle$))/SUM (I).

co-crystallized hpol η with an incoming rCTP positioned opposite template dG in the presence of Ca^{2+} (Table 4). The final Fourier ($2F_o - F_c$) sum electron density map (with a threshold of 1σ) is shown in Fig. 4*A*. The incoming rCTP formed a Watson-Crick base pair with the template dG, but a significant propeller twist was observed. The dihedral angle between the two base planes was 27°. In addition, the base pair was slightly shifted toward the major groove, compared with the dG:dCTP pair at the hpol η active site. Phe-18 was identified as the steric gate residue, and the distance between either 2′-OH or 3′-OH of rCTP and their closest atoms of the Phe-18 side chain was 3.2 Å (Fig. 5). In comparison with the hpol η·dG:dCTP structure (PDB code 4O3N) (29), the position of the phenyl ring of Phe-18 was almost identical. In addition, the distance between the 3′-OH of the primer end (two conformations) to Pα of the incoming rCTP was 4.5 or 4.3 Å, about 1 Å further than that in

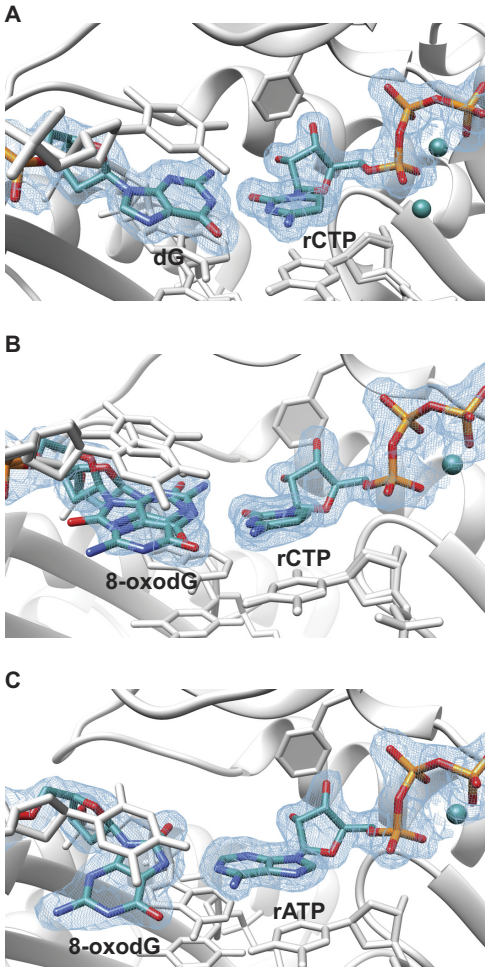

FIGURE 4. **Quality of the final Fourier ($2F_o - F_c$) sum electron density drawn at the 1σ threshold around incoming ribonucleotides and the template base/lesions.** *A*, hpol η·dG:rCTP. *B*, hpol η·(8-oxodG):rCTP. *C*, hpol η·dG:rATP.

the hpol η·dG:dCTP structure (3.5 or 3.3 Å), providing an explanation for the 10^3-fold lower catalytic efficiency of the polymerization reaction (Fig. 5).

hpol η Accommodates 8-oxodG in Two Conformations Opposite the Incoming rCTP—We also crystallized hpol η with an incoming rCTP opposite 8-oxodG (Table 4). The final Fourier ($2F_o - F_c$) sum electron density map is shown in Fig. 4*B*. Noticeably, the electron density of 8-oxodG did not fit either a pure *anti* conformation as seen at the active site of hpol η·(8-oxodG):dCTP or a pure *syn* conformation as in hpol η·(8-oxodG):dATP (29). Instead, the electron density was indicative of two alternative conformations of 8-oxodG. After automated refinement using the program Phenix, the occupancy of 8-oxodG in the *anti* conformation refined to 50%, with the base in the *syn* conformation contributing the other half. In contrast to the dual conformation of 8-oxodG, the incoming rCTP fit the electron density very well, consistent with a single conformation (Fig. 4*B*). When 8-oxodG is in an *anti* conformation, the active site closely resembles that of the hpol η·dG:rCTP complex. Incoming rCTP and 8-oxodG are engaged in a Watson-Crick base pair with formation of a significant propeller twist. The dihedral angles of the bases of the incoming rCTP and 8-oxodG were 29° (*anti* conformation) and 25° (*syn* conformation) (Fig. 6). In the *syn* conformation, 8-oxodG maintained three H-bonds with rCTP as follows: O6 of 8-oxodG H-bonded with N4(H) of rCTP, with a distance of 2.8 Å, and N7(H) of 8-oxodG donated in a bifurcated H-bond to O_2 and N3 of the incoming rCTP, with distances of 3.1 and 3.2 Å, respectively. The O8 atom of 8-oxodG in the *syn* conformation was positioned at 3.6 Å from O2 of rCTP and therefore outside the range for interacting.

With either conformation adopted by 8-oxodG, the 8-oxodG:rCTP pair was shifted toward the major groove compared with the structure of hpol η·(8-oxodG):dCTP (PDB code 4O3P) (29). The closest distance between 2′-OH of rCTP and Phe-18

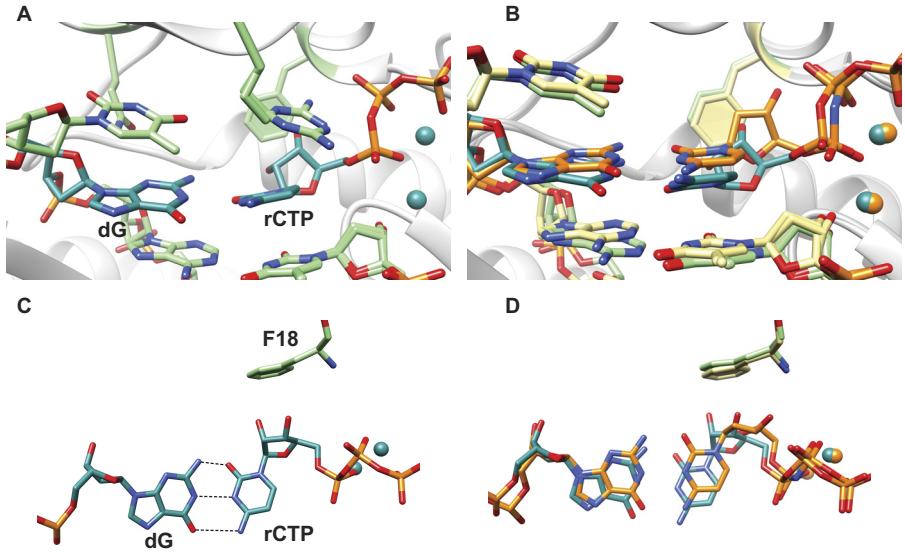

FIGURE 5. **Crystal structure of hpol η inserting rCTP opposite template dG in the presence of Ca^{2+}.** *A*, active site of the hpol η·dG:rCTP complex viewed from the major groove side. *B*, superimposition of the structures of the ternary hpol η·dG·rCTP and hpol η·dG·dCMPNPP (dCTP analog) (PDB code 4O3N) (29) complexes, viewed from the major groove. *C*, dG:rCTP pair at the active site viewed from the *top*. *D*, *top view* of the superimposed active sites in the structures of hpol η·dG:rCTP and hpol η·dG:dCMPNPP complexes. For hpol η·dG:rCTP, the base pair dG:rCTP (as well as Ca^{2+}) are highlighted in *dark cyan*, and the other nucleotides and key residues Arg-61, Gln-38, and Phe-18 are in *light green*. For hpol η·dG:dCTP, both the base pair G:dCMPNPP and Mg^{2+} are shown in *orange*, and the other nucleotides and Phe-18 are shown in *khaki*.

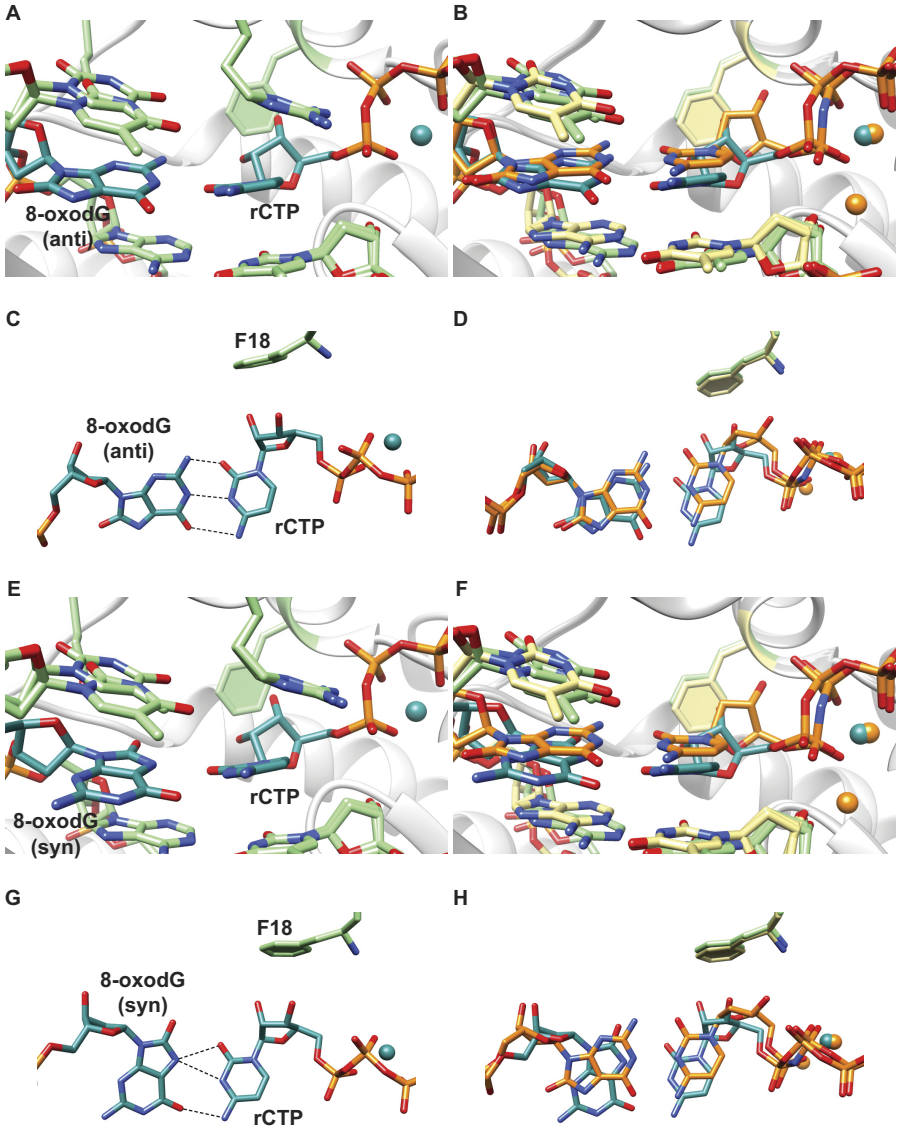

FIGURE 6. **Crystal structure of hpol η inserting rCTP opposite 8-oxodG.** *A*, active site of the hpol η·(8-oxodG *anti*):rCTP complex viewed from the major groove side. *B*, superimposition of the structures of the ternary hpol η-(8-oxodG *anti*):rCTP and hpol η·(8-oxodG):dCMPNPP (PDB code 4O3P) (29) complexes, viewed from the major groove. *C*, (8-oxodG *anti*):rCTP pair at the active site viewed from the top. *D*, *top view* of the superimposed active sites in the structures of the hpol η·(8-oxodG *anti*):rCTP and hpol η·(8-oxodG):dCMPNPP complexes. *E*, active site of the hpol η·(8-oxodG *syn*):rCTP complex viewed from the major groove side. *F*, superimposition of the structures of the ternary hpol η·(8-oxodG *syn*):rCTP and hpol η·(8-oxodG):dCMPNPP (PDB code 4O3P)(29) complexes, viewed from the major groove. *G*, (8-oxodG *syn*):rCTP pair at the active site viewed from the top. *H*, top view of the superimposed active sites in the same structures of the hpol η·(8-oxodG *syn*):rCTP and hpol η·(8-oxodG):dCMPNPP complexes. The *color codes* are the same as in Fig. 5 and H-bonds are *dashed lines*.

was 3.3 Å, and the distance between 3′-OH and the steric gate residue was 3.4 Å. The 3′-OH of the primer end (two conformations) was 4.3 or 4.1 Å away from the Pα of rCTP, whereas the corresponding distance was 3.4 or 3.2 Å in the hpol η·(8-oxodG):dCTP complex, respectively, similar to the relative positions for rCTP and dCTP opposite template dG at the hpol η active site (Fig. 6).

8-oxodG Adopts a syn Conformation in the Pair with the Incoming rATP at the hpol η Active Site—Given that 8-oxodG adopts a *syn*-conformation in the structure of hpol η·(8-oxodG):dATP (PDB code 4O3O) (29), we also examined the orientation of rATP opposite 8-oxodG at the active site of hpol η. The final Fourier ($2F_o - F_c$) sum electron density map around the base pair at the active site is shown in Fig. 4*C*. 8-oxodG indeed adopted a *syn* conformation, but instead of a planar Hoogsteen base pair, a propeller twist of 32° was observed for 8-oxodG:rATP. As a result, the distance between O6 of the lesion and N6 of rATP was 3.7 Å, too long for formation of an H-bond. Because of the propeller twist, 2′-OH of rATP was 3.1 Å away from the closet atom of Phe-18, whereas the closest distance between 3′-OH and the side chain of the steric gate residue was 3.2 Å. In the hpol η·(8-oxodG):rATP complex, 8-oxodG moved closer to the backbone of the template strand, whereas rATP shifted further into the major groove, compared with the hpol η·(8-oxodG):dATP complex. The distance between 3′-OH of the primer end to Pα of rATP was 4.4 Å. By comparison, the corresponding distance in the hpol η·(8-oxodG):dATP complex was 3.3 or 3.1 Å (Fig. 7).

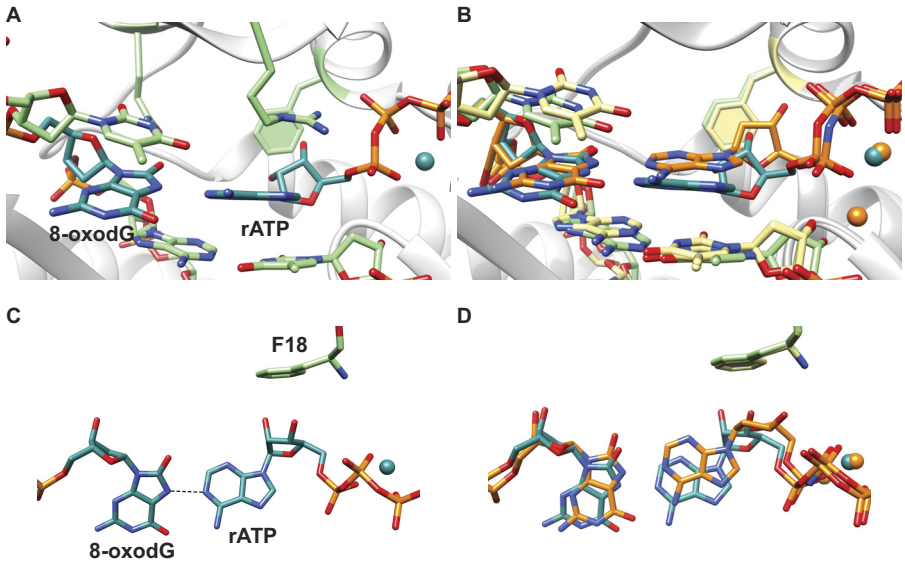

FIGURE 7. **Crystal structure of hpol η inserting rATP opposite 8-oxodG.** *A*, active site of the hpol η·(8-oxodG):rATP complex viewed from the major groove side. *B*, superimposition of the structures of the ternary hpol η·(8-oxodG):rATP and hpol η·(8-oxodG):dAMPNPP (PDB code 4O3O) (29) complexes. *C*, (8-oxodG):rATP pair at the active site viewed from the *top*. *D*, *top view* of the superimposed active sites in the structures of the hpol η·(8-oxodG):rATP and hpol η·(8-oxodG):dAMPNPP complexes. The *color codes* are the same as in Fig. 5.

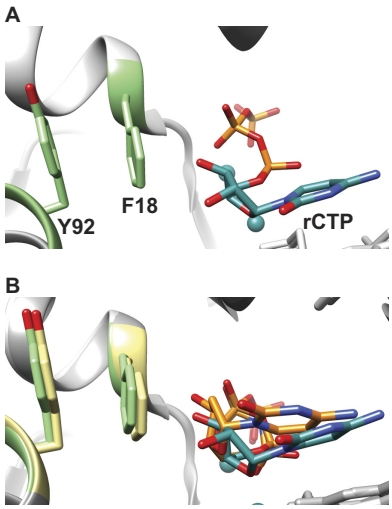

FIGURE 8. **Second line of defense in hpolη: Tyr-92 stabilizes the steric gate residue Phe-18 by π-π interaction.** *A*, steric gate residue Phe-18 and the second line of defense residue Tyr-92 in the hpol η·dG:rCTP complex viewed from the side. *B*, view of Phe-18 and Tyr-92 in the superimposition of the structures of hpol η·dG:rCTP and hpol η·dG:dCMPNPP (PDB code 4O3N) (29). In hpol η·dG:rCTP, Phe-18 and Tyr-92 are shown in *green*, and rCTP and Ca^{2+} are in *dark cyan*. In hpol η·dG:dCMPNPP, Phe-18 and Tyr-92 are shown in *khaki*, and dCMPNPP and Mg^{2+} in shown in *orange*.

Tyr-92 Acts as a Second Line of Defense to Stabilize the Steric Gate Residue Phe-18 at the Active Site of hpol η—Superimpositions of the crystal structure with incoming rNTP and the corresponding structure with incoming dNTP revealed that the side chain of Phe-18 adopts an almost identical position in both cases. Upon closer investigation, a second guard residue, Tyr-92, was identified. The side chain of Tyr-92 is capable of forming a π-π interaction with the phenyl ring of Phe-18, with a distance of about 3.9 Å (Fig. 8). This stacking interaction appears to stabilize the side chain of Phe-18, leaving it in position and preventing the incoming nucleotide from sliding into the minor groove.

To address this hypothesis, we used site-directed mutagenesis to introduce the mutation Y92A in hpol η and examined its activity in steady-state kinetic assays opposite template dG. The catalytic efficiency (k_{cat}/K_m) of the mutant Y92A for dCTP insertion (1.6 μM^{-1} min^{-1}) was 67-fold higher than for rCTP (0.024 μM^{-1} min^{-1}), in comparison with the 770-fold difference for wild-type hpol η (Table 1), indicating that the introduction of the Y92A mutation reduced the sugar discrimination ability of hpol η.

Discussion

Cellular rNTP concentrations are much higher than dNTP concentrations, thus presenting DNA polymerases with a challenge to discriminate against the former (6–9). How DNA polymerases regulate rNTP incorporation has been studied for at least 20 years (6, 8, 16–21). In general, a steric gate residue has been considered to constitute a physical barrier to prevent ribonucleotide incorporation by individual DNA polymerases (10–17). The results of site-directed mutagenesis experiments illustrate the importance of the steric gate effect. For example, the Y39A mutation in hpol ι causes the enzyme to almost totally lose its ability to discriminate between the ribose and deoxyribose sugars (17). Also, the *Sulfolobus solfataricus* DNA polymerase Dpo4 Y12A mutant is capable of incorporating ribonucleotides into primers, and alanine, in place of the steric gate residue Tyr-12, allows space for the 2′-OH of the incoming ribonucleotide, as seen in the x-ray crystal structure (16). A recently published study of yeast pol η shows that mutation of the steric gate residue Phe-35 to an alanine leads to increased ability of ribonucleotide incorporation (47).

2′-OH of the Incoming Ribonucleotide Leads to a Propeller Twist between the Paired Bases at the Active Site of hpol η and Slows the Reaction—We crystallized wild-type hpol η with primer-template DNA duplexes containing either dG or 8-oxodG opposite the incoming rNTP. Interestingly, the extra 2′-OH of the incoming rNTP does not directly point into the

phenyl ring of the steric gate residue. Instead, to avoid close contact, in the structure of rCTP opposite template dG, rCTP undergoes a shift relative to the position of dCTP in the corresponding crystal structure. However, the sugar pucker of the incoming nucleotide is of the C3′-*endo* type in both cases. Because of the shift of rCTP, a significant propeller twist occurs between cytosine of the incoming nucleotide and guanine of the template (Fig. 5). Similar situations were observed in the crystal structures of the hpol η·(8-oxodG):rCTP and hpol η·(8-oxodG):rATP complexes (Figs. 6 and 7). The dihedral angle between the planes of the two bases in the three structures varies between 25 and 32°, compared with 3° in the hpol η·G:dCTP complex (PDB code 403N) (29).

These particular structures accommodated by hpol η are a consequence of its unique, unusually spacious active site that is relatively open on the major groove side. For example, a similar shift by the ribose sugar and the resulting significant propeller twist of the base pair at the active site were not observed in the structure of the wild-type hpol β·DNA:rCTP complex (PDB code 3RH4) (48). Noticeably, in each of the three structures in our study, the distance between the 3′-OH of the primer end to the Pα of the incoming ribonucleotide is increased by 1 Å compared with the corresponding complexes with incoming dNTPs. As a result, the energy barrier for the nucleotidyl transfer reaction is elevated, and the overall reaction rate is reduced by about 3 orders of magnitude.

hpol η Maintains Base Discrimination When the Incoming Nucleotide Is a Ribonucleotide—Our results show that hpol η is still capable of discriminating bases among incoming rNTPs. The Watson-Crick base pair between an incoming rCTP and template dG is maintained, albeit with a propeller twist between bases because of different positioning of sugars of rNTPs relative to dNTPs (Fig. 5). Even with a DNA lesion (8-oxodG or CPD) on the template strand, hpol η still displays relatively high selectivity for the incoming nucleotide as a result of a generally conserved base pairing preference. Thus, it is noteworthy that the catalytic efficiency for rCTP incorporation opposite 8-oxodG is 19-fold higher than that of rATP insertion. By comparison, the change between the catalytic efficiencies of the correct insertion of dCTP opposite the lesion and erroneous insertion of dATP is only 5-fold. In addition, the orientations of 8-oxodG in the template strand vary somewhat in the crystal structures of the hpol η·(8-oxoG):rCTP and hpol η·(8-oxoG)·rATP ternary complexes (Figs. 6 and 7). These results indicate that the incoming rNTP may influence the position and conformation of the template lesion to some extent and therefore affect base selectivity.

Second Line of Defense That Stabilizes the Steric Gate Residue Has Been Observed in Other DNA Polymerases—In our study, we identified Tyr-92 as the second "guard" stabilizing the steric gate residue Phe-18 by π-π interaction, *i.e.* loss of Tyr-92 makes the polymerase an order of magnitude less discriminating. This second line of defense is also seen in some other DNA polymerases, in comparing their structures. For example, hpol ι Tyr-102 acts as the second guard, stacking with the steric gate residue Tyr-39 (17). In hpol κ, Tyr-112 constitutes the steric gate by forming a stacking interaction with Tyr-174 (49). Similarly, in DNA polymerase Dpo4, a pol κ homolog from *S. solfataricus*, the steric gate residue Tyr-12 is accompanied by Tyr-81 that serves as the second line of defense (50). Conversely, the replicative B-family bacteriophage RB69 uses a single DNA polymerase steric gate residue, Tyr-416, packed against an α-helix (19).

Biological Relevance of Ribonucleotide Incorporation by hpol η—Considering that the cellular concentration of rNTPs is 10^1–10^6-fold higher that that of dNTPs (6–9) and the catalytic efficiencies for ribonucleotide insertion are only about 10^3-fold lower than those for deoxynucleotides, it is highly possible that hpol η inserts a considerable amount of ribonucleotides into DNA as part of the various biological processes in which it is involved.

As a member of the DNA polymerase Y-family, one of the most important roles of hpol η is the bypass of lesions during DNA replication. The base selectivity of hpol η mainly depends on the type of the template base/lesion and the flanking DNA sequence (*e.g.* results in Tables 1–3). However, in this study, we also investigated the ability of hpol η to discriminate between ribose and deoxyribose sugars of the incoming nucleotides, especially opposite the DNA lesions 8-oxodG and CPD in the template strand. Judging from our study, the active site of hpol η can simultaneously accommodate a lesion on the template strand and a ribo-sugar of the incoming nucleotide, while still maintaining significant base selectivity.

Author Contributions—Y. S. designed and conducted the experiments, crystallized the proteins, and solved the structures. Y. S., F. P. G., and M. E. conceived the studies, analyzed the results, and wrote the paper.

Acknowledgments—We thank Drs. J. M. Harp, P. S. Pallan, and E. A. Kowal for advice on the x-ray crystallography work. We also thank K. Trisler for assistance in the preparation of the manuscript. Vanderbilt University is a member institution of the Life Sciences Collaborative Access Team at sector 21 of the Advanced Photon Source, Argonne, IL. Use of the Advanced Photon Source at Argonne National Laboratory was supported by the United States Department of Energy, Office of Science, Office of Basic Energy Sciences, under Contract DE-AC02-06CH11357.

References

1. Reijns, M. A., Rabe, B., Rigby, R. E., Mill, P., Astell, K. R., Lettice, L. A., Boyle, S., Leitch, A., Keighren, M., Kilanowski, F., Devenney, P. S., Sexton, D., Grimes, G., Holt, I. J., Hill, R. E., *et al.* (2012) Enzymatic removal of ribonucleotides from DNA is essential for mammalian genome integrity and development. *Cell* **149,** 1008–1022
2. Rydberg, B., and Game, J. (2002) Excision of misincorporated ribonucleotides in DNA by RNase H (type 2) and FEN-1 in cell-free extracts. *Proc. Natl. Acad. Sci. U.S.A.* **99,** 16654–16659
3. Vaisman, A., and Woodgate, R. (2015) Redundancy in ribonucleotide excision repair: competition, compensation, and cooperation. *DNA Repair* **29,** 74–82
4. Sparks, J. L., Chon, H., Cerritelli, S. M., Kunkel, T. A., Johansson, E., Crouch, R. J., and Burgers, P. M. (2012) RNase H2-initiated ribonucleotide excision repair. *Mol. Cell* **47,** 980–986
5. Li, Y. F., and Breaker, R. R. (1999) Kinetics of RNA degradation by specific base catalysis of transesterification involving the 2′-hydroxyl group. *J. Am. Chem. Soc.* **121,** 5364–5372
6. Nick McElhinny, S. A., Kumar, D., Clark, A. B., Watt, D. L., Watts, B. E., Lundström, E. B., Johansson, E., Chabes, A., and Kunkel, T. A. (2010) Genome instability due to ribonucleotide incorporation into DNA. *Nat.*

Chem. Biol. **6,** 774–781
7. Traut, T. W. (1994) Physiological concentrations of purines and pyrimidines. *Mol. Cell. Biochem.* **140,** 1–22
8. Nick McElhinny, S. A., Watts, B. E., Kumar, D., Watt, D. L., Lundström, E. B., Burgers, P. M., Johansson, E., Chabes, A., and Kunkel, T. A. (2010) Abundant ribonucleotide incorporation into DNA by yeast replicative polymerases. *Proc. Natl. Acad. Sci. U.S.A.* **107,** 4949–4954
9. Chabes, A., and Stillman, B. (2007) Constitutively high dNTP concentration inhibits cell cycle progression and the DNA damage checkpoint in yeast *Saccharomyces cerevisiae*. *Proc. Natl. Acad. Sci. U.S.A.* **104,** 1183–1188
10. Joyce, C. M. (1997) Choosing the right sugar: how polymerases select a nucleotide substrate. *Proc. Natl. Acad. Sci. U.S.A.* **94,** 1619–1622
11. DeLucia, A. M., Chaudhuri, S., Potapova, O., Grindley, N. D., and Joyce, C. M. (2006) The properties of steric gate mutants reveal different constraints within the active sites of Y-family and A-family DNA polymerases. *J. Biol. Chem.* **281,** 27286–27291
12. Vaisman, A., Kuban, W., McDonald, J. P., Karata, K., Yang, W., Goodman, M. F., and Woodgate, R. (2012) Critical amino acids in *Escherichia coli* UmuC responsible for sugar discrimination and base-substitution fidelity. *Nucleic Acids Res.* **40,** 6144–6157
13. DeLucia, A. M., Grindley, N. D., and Joyce, C. M. (2003) An error-prone family Y DNA polymerase (DinB homolog from *Sulfolobus solfataricus*) uses a "steric gate" residue for discrimination against ribonucleotides. *Nucleic Acids Res.* **31,** 4129–4137
14. Niimi, N., Sassa, A., Katafuchi, A., Grúz, P., Fujimoto, H., Bonala, R. R., Johnson, F., Ohta, T., and Nohmi, T. (2009) The steric gate amino acid tyrosine 112 is required for efficient mismatched-primer extension by human DNA polymerase κ. *Biochemistry* **48,** 4239–4246
15. Yang, G., Franklin, M., Li, J., Lin, T. C., and Konigsberg, W. (2002) A conserved Tyr residue is required for sugar selectivity in a pol α DNA polymerase. *Biochemistry* **41,** 10256–10261
16. Kirouac, K. N., Suo, Z., and Ling, H. (2011) Structural mechanism of ribonucleotide discrimination by a Y-family DNA polymerase. *J. Mol. Biol.* **407,** 382–390
17. Donigan, K. A., McLenigan, M. P., Yang, W., Goodman, M. F., and Woodgate, R. (2014) The steric gate of DNA polymerase ι regulates ribonucleotide incorporation and deoxyribonucleotide fidelity. *J. Biol. Chem.* **289,** 9136–9145
18. Gosavi, R. A., Moon, A. F., Kunkel, T. A., Pedersen, L. C., and Bebenek, K. (2012) The catalytic cycle for ribonucleotide incorporation by human DNA pol λ. *Nucleic Acids Res.* **40,** 7518–7527
19. Clausen, A. R., Murray, M. S., Passer, A. R., Pedersen, L. C., and Kunkel, T. A. (2013) Structure-function analysis of ribonucleotide bypass by B family DNA replicases. *Proc. Natl. Acad. Sci. U.S.A.* **110,** 16802–16807
20. Clausen, A. R., Zhang, S., Burgers, P. M., Lee, M. Y., and Kunkel, T. A. (2013) Ribonucleotide incorporation, proofreading and bypass by human DNA polymerase δ. *DNA Repair* **12,** 121–127
21. Cavanaugh, N. A., Beard, W. A., and Wilson, S. H. (2010) DNA polymerase β ribonucleotide discrimination: insertion, misinsertion, extension, and coding. *J. Biol. Chem.* **285,** 24457–24465
22. Sale, J. E., Lehmann, A. R., and Woodgate, R. (2012) Y-family DNA polymerases and their role in tolerance of cellular DNA damage. *Nat. Rev. Mol. Cell Biol.* **13,** 141–152
23. Yang, W. (2014) An overview of Y-family DNA polymerases and a case study of human DNA polymerase η. *Biochemistry* **53,** 2793–2803
24. Kunkel, T. A. (2004) DNA replication fidelity. *J. Biol. Chem.* **279,** 16895–16898
25. Inui, H., Oh, K. S., Nadem, C., Ueda, T., Khan, S. G., Metin, A., Gozukara, E., Emmert, S., Slor, H., Busch, D. B., Baker, C. C., DiGiovanna, J. J., Tamura, D., Seitz, C. S., Gratchev, A., *et al.* (2008) Xeroderma pigmentosum-variant patients from America, Europe, and Asia. *J. Invest. Dermatol.* **128,** 2055–2068
26. Masutani, C., Kusumoto, R., Yamada, A., Dohmae, N., Yokoi, M., Yuasa, M., Araki, M., Iwai, S., Takio, K., and Hanaoka, F. (1999) The XPV (xeroderma pigmentosum variant) gene encodes human DNA polymerase η. *Nature* **399,** 700–704
27. Johnson, R. E., Kondratick, C. M., Prakash, S., and Prakash, L. (1999) hRAD30 mutations in the variant form of xeroderma pigmentosum. *Science* **285,** 263–265
28. Biertümpfel, C., Zhao, Y., Kondo, Y., Ramón-Maiques, S., Gregory, M., Lee, J. Y., Masutani, C., Lehmann, A. R., Hanaoka, F., and Yang, W. (2010) Structure and mechanism of human DNA polymerase η. *Nature* **465,** 1044–1048
29. Patra, A., Nagy, L. D., Zhang, Q., Su, Y., Müller, L., Guengerich, F. P., and Egli, M. (2014) Kinetics, structure, and mechanism of 8-oxo-7,8-dihydro-2′-deoxyguanosine bypass by human DNA polymerase η. *J. Biol. Chem.* **289,** 16867–16882
30. Haracska, L., Yu, S. L., Johnson, R. E., Prakash, L., and Prakash, S. (2000) Efficient and accurate replication in the presence of 7,8-dihydro-8-oxoguanine by DNA polymerase η. *Nat. Genet.* **25,** 458–461
31. Patra, A., Zhang, Q., Lei, L., Su, Y., Egli, M., and Guengerich, F. P. (2015) Structural and kinetic analysis of nucleoside triphosphate incorporation opposite an abasic site by human translesion DNA polymerase η. *J. Biol. Chem.* **290,** 8028–8038
32. Haracska, L., Washington, M. T., Prakash, S., and Prakash, L. (2001) Inefficient bypass of an abasic site by DNA polymerase η. *J. Biol. Chem.* **276,** 6861–6866
33. Zhao, Y., Biertümpfel, C., Gregory, M. T., Hua, Y. J., Hanaoka, F., and Yang, W. (2012) Structural basis of human DNA polymerase η-mediated chemoresistance to cisplatin. *Proc. Natl. Acad. Sci. U.S.A.* **109,** 7269–7274
34. Gregory, M. T., Park, G. Y., Johnstone, T. C., Lee, Y. S., Yang, W., and Lippard, S. J. (2014) Structural and mechanistic studies of polymerase η bypass of phenanthriplatin DNA damage. *Proc. Natl. Acad. Sci. U.S.A.* **111,** 9133–9138
35. Vaisman, A., Masutani, C., Hanaoka, F., and Chaney, S. G. (2000) Efficient translesion replication past oxaliplatin and cisplatin GpG adducts by human DNA polymerase η. *Biochemistry* **39,** 4575–4580
36. Bassett, E., King, N. M., Bryant, M. F., Hector, S., Pendyala, L., Chaney, S. G., and Cordeiro-Stone, M. (2004) The role of DNA polymerase η in translesion synthesis past platinum-DNA adducts in human fibroblasts. *Cancer Res.* **64,** 6469–6475
37. Albertella, M. R., Green, C. M., Lehmann, A. R., and O'Connor, M. J. (2005) A role for polymerase η in the cellular tolerance to cisplatin-induced damage. *Cancer Res.* **65,** 9799–9806
38. Chen, Y. W., Cleaver, J. E., Hanaoka, F., Chang, C. F., and Chou, K. M. (2006) A novel role of DNA polymerase η in modulating cellular sensitivity to chemotherapeutic agents. *Mol. Cancer Res.* **4,** 257–265
39. Su, Y., Patra, A., Harp, J. M., Egli, M., and Guengerich, F. P. (2015) Roles of residues Arg-61 and Gln-38 of human DNA polymerase η in bypass of deoxyguanosine and 7,8-dihydro-8-oxo-2′-deoxyguanosine. *J. Biol. Chem.* **290,** 15921–15933
40. Otwinowski, Z., and Minor, W. (1997) Processing of x-ray diffraction data collected in oscillation mode. *Methods Enzymol.* **276,** 307–326
41. McCoy, A. J., Grosse-Kunstleve, R. W., Adams, P. D., Winn, M. D., Storoni, L. C., and Read, R. J. (2007) Phaser crystallographic software. *J. Appl. Crystallogr.* **40,** 658–674
42. Adams, P. D., Afonine, P. V., Bunkóczi, G., Chen, V. B., Davis, I. W., Echols, N., Headd, J. J., Hung, L. W., Kapral, G. J., Grosse-Kunstleve, R. W., McCoy, A. J., Moriarty, N. W., Oeffner, R., Read, R. J., Richardson, D. C., *et al.* (2010) PHENIX: a comprehensive Python-based system for macromolecular structure solution. *Acta Crystallogr. D Biol. Crystallogr.* **66,** 213–221
43. Langer, G. G., Hazledine, S., Wiegels, T., Carolan, C., and Lamzin, V. S. (2013) Visual automated macromolecular model building. *Acta Crystallogr. D Biol. Crystallogr.* **69,** 635–641
44. Murshudov, G. N., Skubák, P., Lebedev, A. A., Pannu, N. S., Steiner, R. A., Nicholls, R. A., Winn, M. D., Long, F., and Vagin, A. A. (2011) REFMAC5 for the refinement of macromolecular crystal structures. *Acta Crystallogr. D Biol. Crystallogr.* **67,** 355–367
45. Emsley, P., Lohkamp, B., Scott, W. G., and Cowtan, K. (2010) Features and development of Coot. *Acta Crystallogr. D Biol. Crystallogr.* **66,** 486–501
46. Pettersen, E. F., Goddard, T. D., Huang, C. C., Couch, G. S., Greenblatt, D. M., Meng, E. C., and Ferrin, T. E. (2004) UCSF Chimera–a visualization system for exploratory research and analysis. *J. Comput. Chem.* **25,** 1605–1612

47. Donigan, K. A., Cerritelli, S. M., McDonald, J. P., Vaisman, A., Crouch, R. J., and Woodgate, R. (2015) Unlocking the steric gate of DNA polymerase η leads to increased genomic instability in *Saccharomyces cerevisiae*. *DNA Repair* **35,** 1–12
48. Cavanaugh, N. A., Beard, W. A., Batra, V. K., Perera, L., Pedersen, L. G., and Wilson, S. H. (2011) Molecular insights into DNA polymerase deterrents for ribonucleotide insertion. *J. Biol. Chem.* **286,** 31650–31660
49. Vasquez-Del Carpio, R., Silverstein, T. D., Lone, S., Swan, M. K., Choudhury, J. R., Johnson, R. E., Prakash, S., Prakash, L., and Aggarwal, A. K. (2009) Structure of human DNA polymerase kappa inserting dATP opposite an 8-oxoG DNA lesion. *PLoS One* **4,** e5766
50. Vaisman, A., Ling, H., Woodgate, R., and Yang, W. (2005) Fidelity of Dpo4: effect of metal ions, nucleotide selection and pyrophosphorolysis. *EMBO J.* **24,** 2957–2967